Interactions of 2,6-substituted purines with purine nucleoside phosphorylase from *Helicobacter pylori* in solution and in the crystal, and the effects of these compounds on cell cultures of this bacterium

Marta Narczyk, Marta Ilona Wojtyś, Ivana Leščić Ašler, Biserka Žinić, Marija Luić, Elżbieta Katarzyna Jagusztyn-Krynicka, Zoran Štefanić & Agnieszka Bzowska

Taylor & Francis
Taylor & Francis Group

RESEARCH PAPER

🔓 OPEN ACCESS Check for updates

Interactions of 2,6-substituted purines with purine nucleoside phosphorylase from *Helicobacter pylori* in solution and in the crystal, and the effects of these compounds on cell cultures of this bacterium

Marta Narczyk[a]* ⓘ, Marta Ilona Wojtyś[a,b]* ⓘ, Ivana Leščić Ašler[c] ⓘ, Biserka Žinić[d] ⓘ, Marija Luić[c], Elżbieta Katarzyna Jagusztyn-Krynicka[b] ⓘ, Zoran Štefanić[c] ⓘ and Agnieszka Bzowska[a] ⓘ

[a]Division of Biophysics, Institute of Experimental Physics, Faculty of Physics, University of Warsaw, Warsaw, Poland; [b]Department of Bacterial Genetics, Institute of Microbiology, Faculty of Biology, University of Warsaw, Warsaw, Poland; [c]Division of Physical Chemistry, Ruđer Bošković Institute, Zagreb, Croatia; [d]Division of Organic Chemistry and Biochemistry, Ruđer Bošković Institute, Zagreb, Croatia

ABSTRACT

Helicobacter pylori represents a global health threat with around 50% of the world population infected. Due to the increasing number of antibiotic-resistant strains, new strategies for eradication of *H. pylori* are needed. In this study, we suggest purine nucleoside phosphorylase (PNP) as a possible new drug target, by characterising its interactions with 2- and/or 6-substituted purines as well as the effect of these compounds on bacterial growth. Inhibition constants are in the micromolar range, the lowest being that of 6-benzylthio-2-chloropurine. This compound also inhibits *H. pylori* 26695 growth at the lowest concentration. X-ray structures of the complexes of PNP with the investigated compounds allowed the identification of interactions of inhibitors in the enzyme's base-binding site and the suggestion of structures that could bind to the enzyme more tightly. Our findings prove the potential of PNP inhibitors in the design of drugs against *H. pylori*.

Introduction

Helicobacter pylori, discovered about 30 years ago[1], is a bacterial pathogen known for its ability to colonise and persist in the human stomach[2], and today affects more than half of the world's population. Although most infections caused by this bacterium are asymptomatic, *H. pylori* is strongly associated with severe diseases of the upper gastrointestinal tract, such as chronic gastritis, peptic ulcer, duodenal ulcer, and gastric cancer, and it is classified as a group I carcinogen[3–6]. There are various recommended treatments for the eradication of *H. pylori*. However, all of them require the use of at least three drugs, as in the first-line triple therapy, and yet they are ineffective in more than 20% of patients, mainly due to the constantly increasing number of strains resistant to one or more antibiotics used in these therapies[7]. *H. pylori* clarithromycin-resistant strains have recently been recognised by WHO as one of the 12 priority pathogens for which novel antibiotics are urgently needed[8]. With a general increase in the consumption of antibiotics, the number of resistant strains is also expected to rise, so a large effort is currently being made to identify new targets for potential drugs that will combat *H. pylori* using different molecular mechanisms than the drugs currently in use[9]. One of the recent examples of an innovative strategy in anti-ulcer treatment is the use of inhibitors of bacterial carbonic anhydrase in combination with probiotic strains[10].

Enzymes belonging to the purine salvage pathway are possible targets of such new drugs because numerous microorganisms, including infectious pathogenic species, are unable to synthesise *de novo* purine nucleotides[11–16]. Therefore, the recovery of purines and purine nucleotides from the environment is for them the only source of these essential DNA and RNA building blocks. Given the importance of purine production and its direct effect on the organisms growth rate, targeting enzymes of the purine salvage pathway became a promising approach to find new drugs against such pathogens. One promising example of the new drug candidate is DADMe-Immucillin-G, a transition state inhibitor of the key enzyme of the purine salvage pathway, purine nucleoside phosphorylase (PNP), which shows clinical potential for treatment of the malaria parasite *Plasmodium falciparum*[16].

PNP, or purine nucleoside orthophosphate ribosyl transferase (EC 2.4.2.1) catalyses the reversible phosphorolytic cleavage of the glycosidic bond of purine ribo and deoxyribonucleosides as follows:

$$(\text{deoxy})\text{purine nucleoside} + \text{orthophosphate} \leftrightarrow \text{purine base}$$
$$+ (2' - \text{deoxy})\text{ribose} - 1 - \text{phosphate}$$
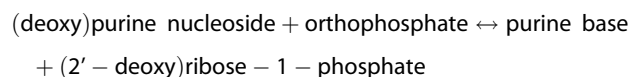
Relatively recently, it was discovered that *H. pylori* also belongs to this class of microorganisms incapable of *de novo* purine synthesis[17]. Nucleoside phosphorylases play a key role in the salvage

---

pathway[18] and, as far as we know, no one has tried to use inhibitors of the PNP to fight *H. pylori* infection. Therefore, in this study, we decided to check the influence of inhibitors of PNP from *H. pylori* on the growth rates of this bacterium in cell culture, and obtain a high-resolution three-dimensional structure of the enzyme-inhibitor complexes to characterise details of the enzyme-ligand interactions. As PNP from *H. pylori* is similar to the *E. coli* PNP[19–21] we decided in the first attempt to check some known inhibitors of the latter enzyme, namely, 2,6-substituted purines[22].

Materials and methods

Materials

Guanosine (Guo) and 2,6-dichloropurine (**2,6-diCl-Pu**, MW 189.00 g/mol) were purchased from Sigma (Saint Louis, MO), magnesium chloride, sodium chloride, sodium dihydrogen phosphate, Tris and Hepes were from Roth (Karlsruhe, Germany), NaOH 99% pure was from POCh (Gliwice, Poland). 7-methylguanosine (m[7]Guo) was synthesised from guanosine according to Jones' and Robins' method[23] involving methyl iodide. This yields the preparation free from sulphate, which as an ion resembling phosphate could bias the results.

PNP from *Helicobacter pylori* strain 26695 (*H. pylori* PNP [HpPNP]) was purified as described previously[20]. Affinity chromatography was the final step of this purification. The Sepharose-Formycin A column, which is necessary for this step, was prepared as described previously for activating Sepharose CL-6B with adenosine and formycin B[24,25].

The synthesis of known compounds 6-benzyloxy-2-chloropurine (**6BnO-2Cl-Pu,** MW 260.68 g/mol), 6-benzylthio-2-chloropurine (**6BnS-2Cl-Pu**, MW 276.74 g/mol), and 6-benzylthiopurine (**6BnS-Pu**, MW 242.3 g/mol)[22,26] is described in the Supplemental Materials.

The 2-chloro-6-benzylthiopurine-2'deoxy-9-ribofuranoside (**6BnS-2Cl-Pu-9dr**, MW 393.87 g/mol) was a kind gift of prof. Zygmunt Kazimierczuk (Warsaw University of Life Sciences, Warsaw, Poland).

Culture reagents – fetal bovine serum (FBS), *Helicobacter pylori* Selective Supplement, Brain Heart Infusion Broth (BHI medium) and Christensen's Urea Broth were from Thermo Fisher Scientific (Waltham, MA). Kanamycin (MW 484.5 g/mol), metronidazole (MTZ; MW 171.15 g/mol), glycerol (MW 92 g/mol), methanol (MW 32.04 g/mol), and dimethyl sulfoxide (DMSO MW 78.13 g/mol) were purchased from Sigma-Aldrich (Saint Louis, MO).

The 24-deep-well 2 ml plates, flat-bottomed for *H. pylori* culture and 96-deep-well microplates were from Nest Scientific Biotechnology (Rahway, NJ). Atmosphere generators were purchased from Mart Microbiology B.V., The Netherlands (Anoxomat Mark II). Microplate reader was from Tecan (Switzerland). Sterile syringe filters with a 0.22 μm pore size were from Merck (Darmstadt, Germany). The *H. pylori* wild-type strain 26695 was obtained from ATCC (Manassas, VA).

All spectrophotometric studies were performed on a double-beam UV/VIS spectrophotometer Cary 100, with thermostated Peltier cell holders (Varian: Agilent Technologies, Mulgrave, Vic., Mulgrave, Australia).

PNP inhibition studies

Usually, the specific activity of PNP is determined with inosine as a substrate, using the assay in which the product of phosphorolysis, hypoxanthine, is oxidised to uric acid in a coupled reaction catalysed by xanthine oxidase[27]. However, for inhibition studies of

PNP from *H. pylori* strain 26695, 7-methylguanosine and guanosine were used as nucleoside substrates to avoid possible inhibition of xanthine oxidase by the tested compounds. Phosphorolysis of these two substrates may be observed using a direct spectrophotometric method as described previously[28,29]. Spectral data for substrate concentration determination and for the activity assays used in this study, are the following: $\varepsilon_{max} = 13{,}650\,M^{-1}cm^{-1}$ for Guo[29], $\varepsilon_{max} = 8500\,M^{-1}cm^{-1}$ for m[7]Guo (at pH 7.0)[28], $\Delta\varepsilon = -4850\,M^{-1}cm^{-1}$ at $\lambda_{obs} = 252$ nm for Guo[29] and $\Delta\varepsilon = -4600\,M^{-1}cm^{-1}$ at $\lambda_{obs} = 258$ nm for m[7]Guo (at pH 7.0)[28].

The enzyme activity was measured in a cuvette with the optical pathlength of 1 or 0.5 cm, so the absorption of the reaction mixture never exceeded 1.2. The reaction volume was 1 or 1.4 mL in 1 and 0.5 cm pathlength cuvettes, respectively. The reaction mixture contained 50 mM HEPES/NaOH buffer pH 7.0, 50 mM phosphate buffer pH 7.0, substrate, and inhibitor (the latter was omitted in the reference reactions).

For HpPNP inhibition studies, the tested compounds were dissolved in methanol, so that the concentration of stock solution was 5 or 10 mM. Inhibitor concentration was calculated based on the weighted amount and confirmed with the absorbance measurement at pH 7.0 in water containing 10% methanol (v/v) and using the extinction coefficients $\varepsilon_{261\,nm} = 10{,}900\,M^{-1}cm^{-1}$ for **6BnO-2Cl-Pu** and $\varepsilon_{299\,nm} = 18{,}000\,M^{-1}cm^{-1}$ for all compounds bearing the 6-BnS substituent[22].

The range of substrate concentration used was 10–280 μM, and the broadest range of inhibitor concentration used was 0–15 μM for **6BnS-Pu** and **2,6-diCl-Pu**, while the lower maximal concentration for other, stronger inhibitors was sufficient to determine the inhibition constants. In the amount added with inhibitors, the effect of methanol on the enzyme activity was measured separately and found to be negligible.

The reaction mixture was pre-incubated for 5 min at 25 °C and enzyme activity (represented here as a change of initial absorbance over time) was measured for the next 2 min. Enzyme velocity was calculated as specific activity in given conditions, expressed in U/mg (U is the amount of enzyme that converts 1 μmol of substrate per minute at 25 °C). Initial velocity was calculated for the period 0.5–1.0 and 1.0–2.0 min from enzyme addition, to check for the linear absorbance change. The average value was taken to determine velocity in the absence and in the presence of inhibitors, v_o and v_i, respectively.

The equations of different types of inhibition were fitted to the experimental data by GraphPad Prism version 8 software (GraphPad Software, La Jolla, CA) to determine the type of inhibition and inhibition constant. The best model was chosen based on the extra sum-of-squares F test for the models with a different number of parameters and on the Akaike's criterion (AIC) for the models that are not nested.

Equations fitted to the data represent uncompetitive (1), non-competitive (2), and mixed type inhibition (3)[30]:

$$v_o(c_o) = \frac{V_{max}\,c_o}{\left(1 + \frac{[I]}{K_{iu}}\right)c_o + K_m} \tag{1}$$

$$v_o(c_o) = \frac{V_{max}\,c_o \left/ \left(1 + \frac{[I]}{K_{in}}\right)\right.}{c_o + K_m} \tag{2}$$

$$v_o(c_o) = \frac{V_{max}\,c_o}{\left(1 + \frac{[I]}{K_{iu}}\right)c_o + \left(1 + \frac{[I]}{K_{ic}}\right)K_m} \tag{3}$$

The latter equation may be rearranged to the form of Equation (8.17) from[31], which is used by the GraphPad Prism program, where $K_{iu} = $ alpha K_{ic}:

$$v_o(c_o) = \frac{V_{max}\ c_o}{\left(1 + \frac{[I]}{\text{alpha}K_{ic}}\right)c_o + \left(1 + \frac{[I]}{K_{ic}}\right)K_m} \qquad (4)$$

Determination of minimal inhibitory concentration (MIC) vs. H. pylori strain 26695

H. pylori ATCC 26695 was maintained as a frozen stock at $-80\,^{\circ}$C in BHI medium (37 g/L) supplemented with 20% glycerol and 10% FBS. Bacteria were grown on BHI agar plates containing 10% FBS and 1% *H. pylori* Selective Supplement under microaerophilic conditions at 37 $^{\circ}$C for 3 d. Microaerophilic conditions were generated using an atmosphere generator Anoxomat Mark II. Overnight liquid culture of *H. pylori* was grown by shaking at 37 $^{\circ}$C under microaerophilic conditions in BHI medium supplemented with 10% FBS and 1% *H. pylori* Selective Supplement. Subsequently, double strengthened BHI medium was supplemented with 20% FBS and 2% *H. pylori* Selective Supplement.

The experiment was carried out in 24-deep-well 2 mL flat-bottomed plates, all in a final volume of 500 μL. In each well, 2-fold serial dilutions of inhibitors (in a final volume) and an equal volume of inoculated double-strength BHI were added (approximately 0.05 optical density OD_{600} which corresponds to 4×10^4 CFU/mL in a final volume). Kanamycin 25 μg/mL[32] was used as a positive control, while Milli-Q water and BHI medium untreated with *H. pylori* were used as negative controls. *H. pylori* was grown on the plates with shaking (120 rpm) at 37 $^{\circ}$C under microaerophilic conditions and OD_{600} of samples was measured in the microplates at the start of the experiment and after 4, 8, and 24 h for minimal inhibitory concentration (MIC) determination[33]. In the negative control after 24 h incubation, hence at the end of the experiment, OD_{600} typically was in the range of 1.2–1.4, which corresponds to about 10^6 CFU/mL. This method was further improved by applying the approach of Knezevic et al.[34], which checks if the change in OD_{600} comes from viable *H. pylori* cells. The equal volume of double strength Christensen's urea broth was added into wells after incubation, and the plates were additionally incubated for 4 h in an aerobic atmosphere at 37 $^{\circ}$C. During the incubation, in wells with viable *H. pylori* urease produced by the bacteria converted urea into ammonia and carbon dioxide, changing the pH and colour of a phenol red indicator in the medium (from orange to purple)[34]. The MIC is defined as the lowest concentration of a compound that inhibits visible growth (absence of colour change), compared with the growth in the controls (presence of colour change), which in the OD_{600} monitoring method corresponds to inhibition comparable to that in the positive control with 25 μg/mL kanamycin (i.e. % of inhibition of bacterial growth is 90% or higher). All experiments were performed in three repetitions.

Checkerboard assay

The combined antimicrobial activity of **6BnS-2Cl-Pu** with MTZ was determined against *H. pylori* 26695 strain using the checkerboard assay[35]. Concentrations below MIC were tested. A concentration gradient used for the **6BnS-2Cl-Pu** was 3.0–10.0 μg/mL. The range of MTZ concentrations was chosen based on MIC given in EUCAST[36], 8 μg/mL. However, in our case, *H. pylori* 26695 strain, already with 2 μg/mL we observed 89–92% inhibition (Table 3). The range of concentrations of the tested compounds was prepared in test tubes in such a way as to obtain twice the test concentrations when testing the activity of **6BnS-2Cl-Pu** or MTZ

alone and four-fold test concentrations when testing the combination of both.

The experiment with controls was prepared in the same way as described previously in the section "*Determination of minimal inhibitory concentration (MIC) vs. H. pylori strain 26695.*" The experiment was carried out in 24-deep-well 2 mL flat-bottomed plates, all in a final volume of 500 μL. In each well, where the activity of **6BnS-2Cl-Pu** or MTZ alone was tested, 250 μL of one or the other substance in twice the test concentration and an equal volume of inoculated double-strength BHI were added (approximately 0.05 optical density OD_{600} which corresponds to 4×10^4 CFU/mL in a final volume). Whereas to the remaining wells, in which the interactions in the antimicrobial activity were determined, 125 μL of each **6BnS-2Cl-Pu** and MTZ in four-fold test concentration with 250 μL of inoculated double-strength BHI were added (approximately 0.05 optical density OD_{600} which corresponds to 4×10^4 CFU/mL in a final volume). The plates were incubated with shaking (120 rpm) at 37 $^{\circ}$C under microaerophilic conditions and OD_{600} of samples was measured in the microplates after 4, 8, and 24 h for MIC determination. The MIC values were confirmed using Christensen's urea broth. All experiments were performed in three repetitions.

The interaction between the tested compounds was determined by calculating the fractional inhibitor concentration index (FICI) as $FICI = (MIC_A/MIC_a) + (MIC_B/MIC_b)$, where $MIC_A = MIC$ of substance a, in the presence of substance b; $MIC_a = MIC$ of substance a, applied as a single agent; $MIC_B = MIC$ of substance b, in the presence of substance a, and $MIC_b = MIC$ of inhibitor b, applied as a single agent. The results were interpreted as a synergistic effect if the FICI was <0.5; as an additive effect if $0.5 < FICI < 1$; a neutral effect if $1 < FICI < 4$; and as an antagonistic effect if the FICI was >4[37].

Preparation of solutions of tested compounds for H. pylori cell culture inhibition test

For checking the influence of the PNP inhibitors used in this study on the *H. pylori* cell culture growth, 10 mM stocks of **6BnO-2Cl-Pu**, **6BnS-2Cl-Pu**, **6BnS-Pu**, and **6BnS-2Cl-Pu-9dr** were prepared in DMSO, while 10 mM stock of **2,6-diCl-Pu** was prepared in milli-Q water. In some cases, 15 mM stock of **6BnS-2Cl-Pu** was used. Stocks in DMSO were diluted with water, so that the DMSO content in the final solution used in the cell culture experiments in most cases did not exceed 5% (v/v). Hence, after two-fold dilution of the bacterial culture, the DMSO concentration in the experiment was a maximum 2.5% (in some cases 3.5%). It was independently checked that concentration up to 2.5% is almost neutral for the growth of *H. pylori,* while higher DMSO content inhibits *H. pylori* growth (Figure S5). Nevertheless, in each experiment, the inhibition by DMSO was always checked to see its effect in this particular case, and compared with the effect of the HpPNP inhibitor tested. It was necessary as inhibition observed for the particular % of DMSO differs slightly among the experiments. Two-fold serial dilutions with water prepared from the 10 mM **2,6-diCl-Pu** stock show no precipitated compound, as this purine derivative exhibits good solubility in water. By contrast, upon dilution with water, also depending on the final concentration planned to obtain, in the case of the four other tested compounds, **6BnO-2Cl-Pu**, **6BnS-2Cl-Pu**, **6BnS-Pu**, and **6BnS-2Cl-Pu-9dr**, a part of the dissolved inhibitor precipitated out of the solution. To overcome this problem, such solutions were filtered through sterile syringe filters with a 0.22 μm pore size and the supernatants thus obtained were tested in *H. pylori* culture. The

concentration of the tested compounds present in the final filtered solutions was measured spectrophotometrically using the extinction coefficients shown in the section "*PNP inhibition studies*." Second, the parallel approach used to determine the MIC of these compounds was to use unfiltered supernatants in which part of the compound was in solution and part in the form of precipitate (Table S1).

Crystallisation, data collection, and structure determination

Crystals of HpPNP complexes were obtained by the hanging-drop vapour diffusion method. The drops involved were set up with 1 or 2 μL of protein complexed with ligands and 1 or 2 μL of reservoir solution, whereas the reservoir volume was 700 μL. The crystallisation conditions were identified previously[21] and contained 0.02 M MgCl$_2$, 0.1 M Tris–HCl pH 7.0–7.6, 9–13% PEG 8000. For crystallisation, HpPNP (9–10 mg/mL in 50 mM Tris–HCl buffer, pH 7.6) was mixed with ligands (0.5–0.6 mM phosphate and 0.5–1.4 mM 2,6-substituted purine) and kept for 30 min before setting up the crystallisation drops. The complex of HpPNP with **6BnS-2Cl-Pu** was obtained by mixing protein with the respective nucleoside **6BnS-2Cl-Pu-9dr** and allowing the phosphorolysis to occur. The complex of HpPNP with **2,6-diCl-Pu** was obtained by soaking and using different crystallisation conditions, namely, 0.2 M imidazole, pH 7.0 and PPG 400. The ligand was added as a powder to the drop with already existing crystals and stayed for 3 d before freezing.

Data collection for all structures was done at the XRD1 beamline of the Elettra synchrotron, Trieste, Italy using the Dectris Pilatus 2 M detector. The data collection and refinement parameters for the structures are summarised in Table 1. The data were integrated using the XDS program[38]. All structures were solved by molecular replacement using the Molrep program[39] and using the structure of *H. pylori* PNP (PDB code 5LU0[20]) as a model, and the ligands were located in the difference maps. The models were then refined using the phenix.refine routine from the Phenix package[40]. Coordinates and structure factors were deposited in the Protein Data Bank with the following PDB codes: 7OOY for **6BnS-2Cl-Pu,** 7OOZ for **6BnO-2Cl-Pu**, 7OPA for **6BnS-Pu,** and 7OP9 for **2,6-diCl-Pu**. The figures of X-ray structures were made using Pymol[41].

Results and discussion

Inhibition of the H. pylori purine nucleoside phosphorylase

Inhibition of *H. pylori* PNP by 2- and/or 6-substituted purines, and by a 2′-deoxyriboside of 2-chloro-6-benzylthiopurine (Figure 1), was studied with 7-methylguanosine as variable substrate at saturating phosphate concentration (50 mM). Inhibition model and inhibition constants were determined and are depicted in Table 2. Data are also shown in Figures 2 and 3 and Figure S4. In most cases studied, when the Michaelis–Menten equation was fitted to each kinetic trace separately, it was found that both parameters, Michaelis constant, K_m, and the maximal velocity, V_{max}, significantly change when the inhibitor is present. Therefore, the mixed inhibition model was fitted

Table 1. Data collection and refinement statistics.

Structure	6BnS-2Cl-Pu	6BnO-2Cl-Pu	6BnS-Pu	2,6-diCl-Pu
Resolution range	35.9–1.9 (1.97–1.9)[a]	35.9–1.7 (1.76–1.7)	46.35–2.0 (2.07–2.0)	42.59–1.5 (1.55–1.5)
Space group	$P\,2_1\,3$	$P\,2_1\,3$	$P\,2_12_12_1$	$P\,1$
Unit cell				
a, b, c (Å)	113.6, 113.6, 113.6	113.7, 113.7, 113.7	67.6, 139.0, 318.7	93.4, 93.4, 95.4
α, β, γ (°)	90, 90, 90	90, 90, 90	90, 90, 90	81.9, 79.3, 60.1
Total reflections	433,440 (40977)	465,820 (44846)	2,504,977 (186198)	1,079,039 (98731)
Unique reflections	38,724 (3843)	54,014 (5331)	202,884 (19800)	419,695 (38205)
Multiplicity	11.2 (10.7)	8.6 (8.4)	12.3 (9.4)	2.6 (2.6)
Completeness (%)	99.97 (99.97)	99.93 (99.61)	99.83 (98.78)	94.95 (86.85)
Mean $I/\sigma(I)$	7.83 (1.14)	12.18 (1.53)	9.85 (0.76)	9.13 (1.78)
Wilson B-factor	20.88	19.04	36.70	13.35
R_{merge}	0.32 (2.1)	0.12 (1.27)	0.18 (2.18)	0.09 (0.52)
R_{meas}	0.33 (2.2)	0.13 (1.36)	0.19 (2.30)	0.11 (0.66)
R_{pim}	0.10 (0.69)	0.04 (0.46)	0.05 (0.73)	0.07 (0.39)
$CC_{1/2}$	0.99 (0.48)	0.99 (0.60)	0.99 (0.57)	0.99 (0.54)
CC^*	0.99 (0.80)	0.99 (0.87)	0.99 (0.85)	0.99 (0.84)
Reflections used in refinement	38,720 (3843)	54,008 (5330)	202,855 (19799)	417,539 (38185)
Reflections used for R_{free}	1992 (197)	1989 (197)	1999 (196)	2013 (187)
R_{work}	0.16 (0.26)	0.16 (0.28)	0.23 (0.39)	0.17 (0.31)
R_{free}	0.20 (0.31)	0.19 (0.31)	0.28 (0.43)	0.20 (0.37)
CC_{work}	0.97 (0.78)	0.97 (0.82)	0.92 (0.34)	0.97 (0.84)
CC_{free}	0.96 (0.77)	0.96 (0.83)	0.90 (0.43)	0.97 (0.70)
Number of non-hydrogen atoms	4106	4104	22,971	25,064
Macromolecules	3627	3653	21,616	21,765
Ligands	79	146	198	214
Solvent	400	305	1157	3085
Protein residues	466	466	2796	2796
RMS(bonds)	0.009	0.008	0.008	0.006
RMS(angles)	1.03	1.01	1.02	0.93
Ramachandran favoured (%)	96.75	96.97	94.59	96.89
Ramachandran allowed (%)	3.25	3.03	4.87	3.11
Ramachandran outliers (%)	0.00	0.00	0.54	0.00
Rotamer outliers (%)	1.26	1.25	3.79	0.46
Clashscore	5.20	4.02	10.46	4.23
Average B-factor	24.02	23.22	44.93	19.03
Macromolecules	22.92	22.04	45.06	17.66
Ligands	29.32	32.70	47.49	18.50
Solvent	32.93	32.86	41.99	28.74

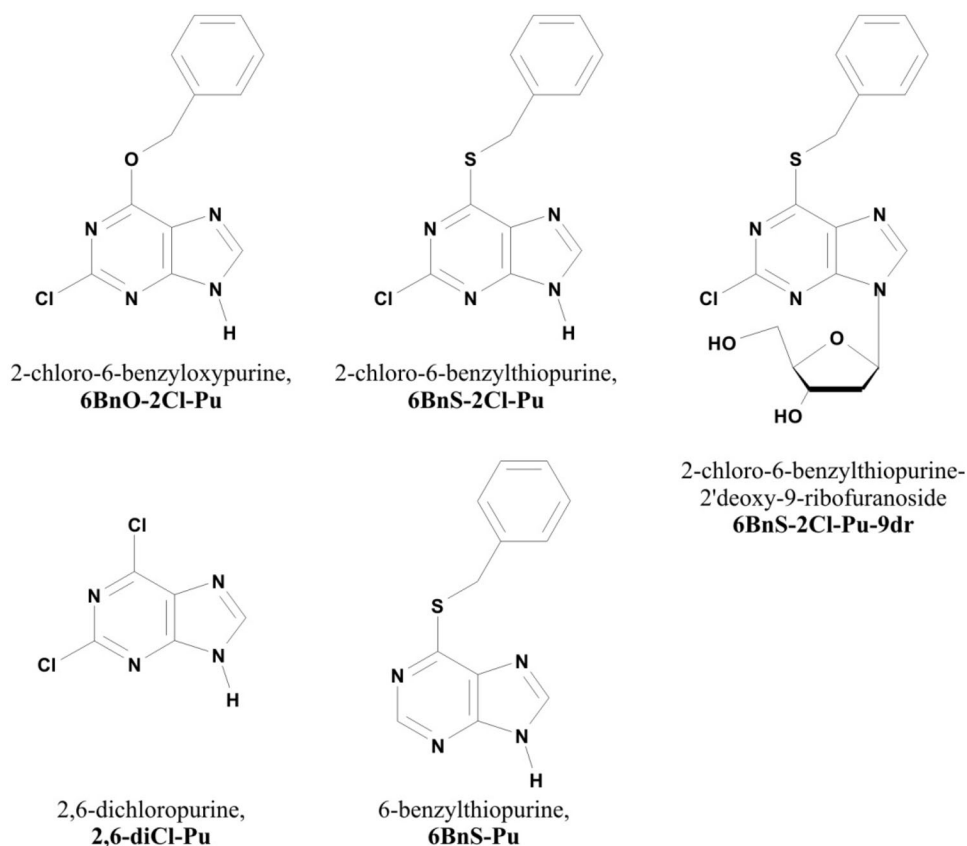[a]Statistics for the highest-resolution shell are shown in parentheses.

Figure 1. Structure of purine derivatives used in this study.

Table 2. Inhibition properties of some purines substituted at positions 2 and/or 6, and deoxyriboside of one of them, *vs. H. pylori* PNP.

Inhibitor	K_{in} [μM]	K_{ic} [μM]	K_{iu} [μM]	alpha[a]
2,6-Dichloropurine[b]	22.2 ± 1.4	–	–	–
2,6-Dichloropurine	–	20.0 ± 4.9	23.5 ± 3.5	1.17 ± 0.44
6-Benzylthiopurine[b]	7.9 ± 0.4	–	–	–
6-Benzylthiopurine	–	7.5 ± 1.3	8.1 ± 0.7	1.07 ± 0.27
2-Chloro-6-benzyloxypurine[c]	–	18.3 ± 7.3	4.6 ± 0.5	0.25 ± 0.12
2-Chloro-6-benzyloxypurine	6.5 ± 0.4	–	–	–
2-Chloro-6-benzyloxypurine	–	–	3.8 ± 0.3	–
2-Chloro-6-benzylthiopurine[d]	–	–	1.8 ± 0.2	–
2-Chloro-6-benzylthiopurine	–	13.2 ± 10.7	2.1 ± 0.3	0.16 ± 0.15
2-Chloro-6-benzylthiopurine-2′deoxy-9-ribofuranoside[c]	–	6.2 ± 2.4	2.9 ± 0.5	0.47 ± 0.24
2-Chloro-6-benzylthiopurine-2′deoxy-9-ribofuranoside[c,e]	–	12.6 ± 5.7	2.0 ± 0.2	0.16 ± 0.08

Data were obtained at 25 °C, in the 50 mM Hepes/NaOH buffer pH 7.0, at saturating phosphate concentration of 50 mM. If not otherwise indicated, m⁷Guo was used as variable substrate.
[a]Alpha = K_{iu}/K_{ic}, see Equation (3) and (4) in Materials and methods.
[b]Non-competitive inhibition model is the best.
[c]Mixed inhibition model is the best.
[d]Uncompetitive inhibition model and mixed type inhibition have similar probability. Due to poor solubility of the compound, data are limited to low inhibitor concentration, errors of K_{ic} and parameter alpha are big, so it is not possible to unequivocally decide which inhibition model is actually better, uncompetitive or mixed.
[e]Inhibition *vs*. guanosine as variable substrate.

globally to the whole data set for each compound, and compared with the fitting of the simpler models, competitive, non-competitive, and uncompetitive to the same data set.

For **2,6-diCl-Pu** and **6-BnS-Pu**, the non-competitive inhibition model is sufficient to describe the data (Figure 2) properly, and the inhibition constants were found to be (22.2 ± 1.4) μM and (7.9 ± 0.4) μM, respectively, showing that benzylthio substituent at position 6 replacing the chlorine atom, enhances the interaction of the purine analogue with the enzyme.

In the case of the **6BnO-2Cl-Pu**, a mixed inhibition model is necessary to describe the data obtained, and fitting of this model

(Figure 3, left panel) yielded the competitive inhibition constant K_{ic} = (18.3 ± 7.3) μM and the uncompetitive inhibition constant K_{iu}=(4.6 ± 0.5) μM (alpha = K_{iu}/K_{ic}=0.25 ± 0.12). The same model is the best in the case of **6BnS-2Cl-Pu-9dr** (Figure S4, right panel), and the appropriate parameters fitted are K_{ic}=(6.2 ± 2.4) μM and uncompetitive inhibition constant K_{iu}=(2.9 ± 0.5) μM (alpha = K_{iu}/K_{ic}=0.47 ± 0.24) suggesting that sulphate atom replacing oxygen atom at position 6, acting as a linker between purine ring and benzyl ring, has a positive effect yielding stronger inhibition. To confirm this, we repeated the experiment with guanosine as a substrate undergoing phosphorolysis (Figure S4, left panel), and
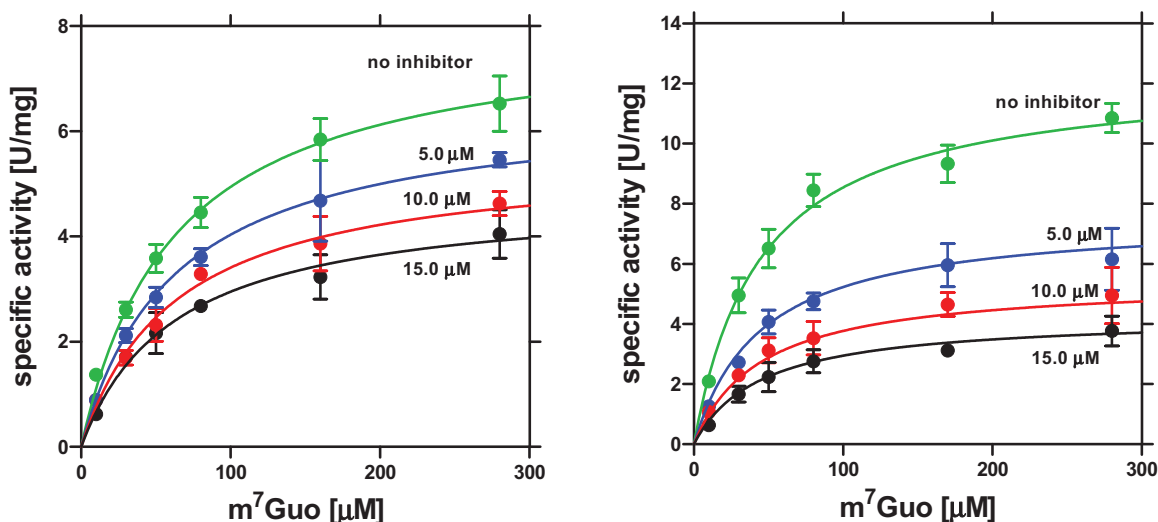
Figure 2. Inhibition of *H. pylori* PNP at 25 °C, 50 mM Hepes/NaOH, pH 7.0, by **2,6-diCl-Pu** (left) and by **6-BnS-Pu** (right) with m^{7}Guo and 50 mM phosphate as substrates. Initial velocity, v_o, vs. variable substrate concentration (m^{7}Guo), with no inhibitor added (green circles) and with several various concentrations of the inhibitor are shown; error bars represent SD; solid lines represent global fitting of the non-competitive inhibition model.
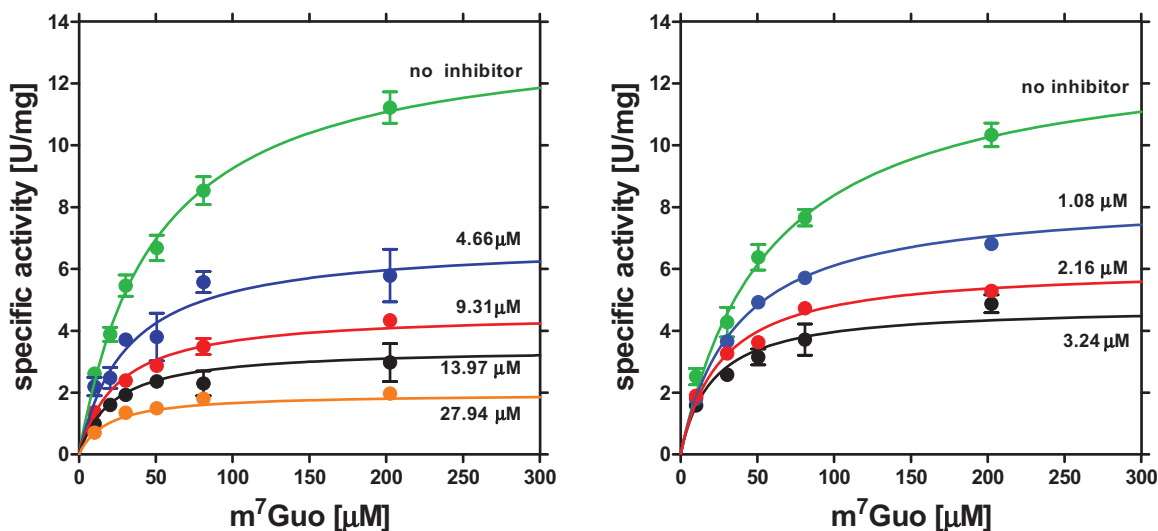
Figure 3. Inhibition of *H. pylori* PNP at 25 °C, 50 mM Hepes/NaOH, pH 7.0, by **6BnO-2Cl-Pu** (left) and by **6BnS-2Cl-Pu** (right) with m^{7}Guo and 50 mM phosphate as substrates. Initial velocity, v_o, vs. variable substrate concentration (m^{7}Guo), with no inhibitor added (green circles) and with several various concentrations of the inhibitor are shown; error bars represent SD; solid lines represent the global fitting of the mixed inhibition model.

the respective parameters describing inhibition were found to agree in the 3σ test (Table 2).

6BnS-2Cl-Pu (Figure 3, right panel) turned out to be the strongest inhibitor, and the uncompetitive model gives $K_{iu}=(1.8 \pm 0.2)$ μM, but this and the mixed inhibition model have almost the same probability. Since the solution of **6BnS-2Cl-Pu** in methanol partially precipitated upon adding to the reaction mixture (prepared in water), the data points obtained for the inhibitor concentration higher than 6 μM (6.48 and 9.72 μM, not shown) were excluded from the global fit. Therefore, the inhibition is probably a mixed type, but the poor solubility of the compound precludes measurements with higher inhibitor concentration, which could help to distinguish between models. Mixed type inhibition by such type of compounds was also previously reported for the *E. coli* PNP[22], which is very similar to the *H. pylori* PNP[20,21,42].

Inhibition of *H. pylori* cell culture

Encouraged by the fact that some of the tested compounds turned out to be relatively potent inhibitors of PNP from the *H. pylori* 26695 strain, we decided to check the effect of these compounds on the proliferation of cell cultures of this bacterium. We started with **2,6-diCl-Pu**, which is well soluble in water. We have found that it is effective in inhibiting *H. pylori* 26695 strain proliferation, but the MIC necessary to stop bacteria cell culture growth is rather high, 473 μg/mL, which corresponds to 2.5 mM (Figure S5, Table 3).

Due to the benzyl ring at position 6, the four other compounds studied are not well soluble in water but in organic compounds like, for example, methanol or DMSO. Methanol is too volatile to be used in such an assay. Therefore, we first checked the impact of DMSO on *H. pylori* 26695 strain growth, and we observed that

Table 3. Minimal inhibitory concentration (MIC) values, and inhibition obtained at the maximal solubility in 3.5% DMSO of the compounds tested in this study, against *H. pylori* 26695 strain cell cultures.

| Inhibitor | MW | MIC[a] | | Maximal solubility | | % of *H. pylori* cell culture inhibition at inhibitor maximal solubility |
		[μg mL^{-1}]	[μM]	[μg mL^{-1}]	[μM]	
DMSO	78.13	–	–	55.0[b]	–	60[e]
				38.5[b]	–	26[e]
				27.5[b]	–	0[e]
2,6-diCl-Pu	189.00	473	2500	236	1250	93
6BnO-2Cl-Pu	260.68	–	–	25[c]	95[c]	35
				91[d]	350[d]	75
6BnS-2Cl-Pu	276.74	69[d]	250[d]	11.1	40	92
6BnS-Pu	242.3	48[d]	200[d]	21	85	83
6BnS-2Cl-Pu-9dr	393.87	79[d]	200[d]	4.3[c]	10.8[c]	5
metronidazole	171.15	8[f]	47	2[g]	12[g]	89–92
kanamycin	484.5	0.5–64[f]	1.1–132	25[g]	52[g]	92–96
BHI medium untreated with *H. pylori*	–	–	–	–	–	95[h]

The results are presented as the mean of three repetitions (see Materials and methods).
[a]MIC is the minimal concentration used in the series of 2-fold dilutions that gave full inhibition of *H. pylori* cell culture growth, i.e. comparable to that observed for the positive control with 25 μg/mL kanamycin, i.e. by 92–96%.
[b]These correspond to 5%, 3.5%, and 2.5% (v/v), respectively, and in this case, this is not the maximal solubility; DMSO density 1.1 g/cm^3.
[c]It was a maximal concentration possible to obtain in given conditions (at this concentration saturation was observed, see Table S1).
[d]Inhibitor partially precipitated, so actual concentration of dissolved compound is lower.
[e]In each experiment, the inhibition by DMSO was always checked to see its effect in this particular case, and compared with the effect of the HpPNP inhibitor tested. It was necessary as inhibition observed for the particular % of DMSO differs slightly among the experiments.
[f]MTZ according to[36], kanamycin according to[32].
[g]In this case this concentration is not the maximal solubility.
[h]In this case there is no *H. pylori*, so the value shown is treated as a negative control.

DMSO at a concentration up to 2.5% (v/v) inhibits the growth of *H. pylori* only slightly (Figure S5). Therefore, when examining the effect of DMSO-soluble compounds on the growth of *H. pylori*, we did not exceed the latter concentration of this solvent, and we always included DMSO in each experiment for direct comparison (see Materials and methods).

When the stocks of **6BnO-2Cl-Pu**, **6BnS-Pu**, **6BnS-2Cl-Pu**, and **6BnS-2Cl-Pu-9dr** in DMSO were diluted with water to obtain appropriate concentrations, all four compounds were partially precipitated, so we decided to investigate in parallel the effect of (i) the solution of the partially precipitated compounds, and (ii) their supernatants obtained by filtering of the former (see Materials and methods). The actual concentration of the inhibitors in the supernatants was determined by performing UV spectra of several times diluted supernatants, and the absorbance at 261 nm (maximum) in the case of **6BnO-2Cl-Pu**, 290 nm in the case of **6BnS-Pu** and 299 nm (maximum) in the case of **6BnS-2Cl-Pu** and **6BnS-2Cl-Pu-9 dr**, was used to calculate the concentration of the tested compound, and these data are shown in Table S1. It was noticed that for the higher planned concentrations a significant part of each compound precipitated out of the solution, so the actual concentrations of the obtained supernatants turned out to be much lower than intended.

The maximal tested concentration of the fully dissolved **6BnO-2Cl-Pu** was 0.095 mM. It inhibits but not completely only by about 35%, the growth of *H. pylori* 26695 strain (Figure S5, Table 3). However, if the partially precipitated solution was used, an inhibition about 75% was observed, with **6BnO-2ClPu** prepared as 0.35 mM but partially precipitated (Table 3). These results suggest that the bacteria uptake the dissolved inhibitor, and the precipitated solid material is gradually dissolved to maintain the equilibrium.

Even more promising results were obtained with **6BnS-2Cl-Pu**, for which the maximal tested concentration of the fully dissolved compound, 0.040 mM, yielded 92% inhibition of *H. pylori* 26695 cell culture growth, while the solution prepared as 0.25 mM but partially precipitated, led to the full inhibition (Figure 4, Table 3).

The maximal tested concentration of the fully dissolved **6BnS-2Cl-Pu-9dr** was 10.8 μM (see Table S1). The compound in this

concentration has a very small effect on bacterial growth. However, with **6BnS-2Cl-Pu-9dr** prepared as 200 μM but partially precipitated, complete inhibition of *H. pylori* 26695 strain growth is observed (Figure S5, Table 3). Moreover, prepared as 200 μM but partially precipitated **6BnS-Pu** completely inhibited the growth of *H. pylori* 26695 strain, while the maximal concentration of the fully dissolved **6BnS-Pu** (85 μM) yielded 83% inhibition (Figures 4 and 5, Table 3).

The above results show that the investigated compounds can inhibit *H. pylori* cell culture growth. The urease test with the Christensen's urea broth confirms that monitored *H. pylori* cells were viable (see the example of such data (Figure 5)).

The best PNP inhibitor, **6BnS-2Cl-Pu** almost completely stops bacterial growth (by 92%, hence comparable to MTZ and kanamycin, see Table 3) at 40 μM concentration, maximal to obtain in given conditions. Complete growth inhibition occurs when 0.25 mM solution is used. However, at this concentration, the inhibitor partially precipitates, and while the dissolved material penetrates into bacterial cells, the present solid material maintains the equilibrium concentration of the dissolved inhibitor at the maximum possible level, which appears to be sufficient to arrest the growth of *H. pylori* cell culture (Figure 4, Table 3).

Combined antimicrobial effect of 6BnS-2Cl-Pu and metronidazole

We have performed the checkerboard test with the most promising PNP inhibitor, **6BnS-2Cl-Pu**, with one of the antimicrobials used in anti *H. pylori* therapies, MTZ, to check possible additive or synergistic effects of this combination. Data displayed in the upper panel of Figure 6 suggest an additive effect of MTZ and **6BnS-2Cl-Pu**, because FICI determined based on this data (taking MIC of MTZ 2 μg/mL and MIC for **6BnS-2Cl-Pu** 11.1 μg/mL, see Table 3) is 0.83, hence between 0.5 and 1.0. However, as the solution of **6BnS-2Cl-Pu** contains DMSO (typically 1% per 3 μg/mL of **6BnS-2Cl-Pu**, maximum was 3.5%), the effect of MTZ solution containing 3.5% DMSO (Figure 6 lower panel, second row), and DMSO alone, 3.5% and 2.3% was also checked. Lower DMSO concentration, 2.3% does not affect *H. pylori* cell culture growth, while
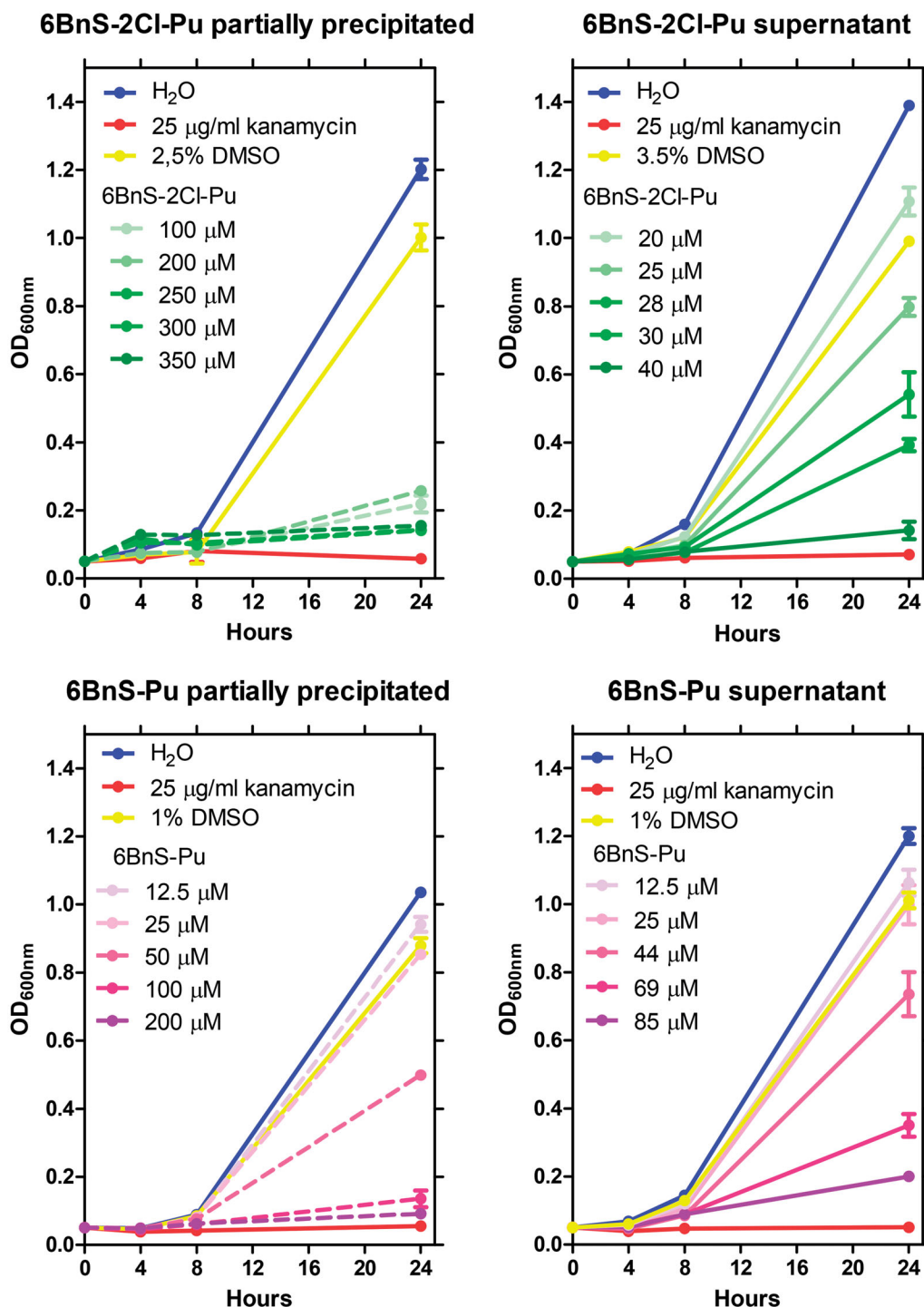
Figure 4. Growth curves of *H. pylori* 26695 strain in the presence of various concentrations of **6BnS-2Cl-Pu** (upper panels) and **6BnS-Pu** (lower panels). Left panels – effects of partially precipitated stocks of the inhibitors, hence the actual concentration of dissolved inhibitor is lower. Right panels – effect of filtered stocks (supernatants). The effect of stocks (supernatants) of the particular tested compound (left panels), and the respective filtered solution of these stocks (right panels) are marked with the same colour, with the dashed and solid lines, respectively.

3.5% yields 26% inhibition. Therefore FICI might be actually higher, and it is possible that the combined effect of MTZ and **6BnS-2Cl-Pu** is neutral (FICI in the range 1.0–4.0[37]), not additive.

Although the poor solubility in water of purines substituted with a benzyl ring makes some problems determining MIC, the effects of these compounds on the proliferation of *H. pylori* cell cultures are very encouraging. To check how interactions with the target enzyme may be improved, we have determined the X-ray structure of *H. pylori* PNP complexes with the four purine analogues described above.

Structure of the *H. pylori* PNP complexes with 2,6-substituted purines

The PNP from *H. pylori* is a homo-hexamer consisting of six identical chains, each having 233 amino acids. The monomers in the hexamer are paired into three dimers, connected by a 2-fold symmetry operation passing between monomers. The complete hexamer is generated by a 3-fold symmetry axis perpendicular to the plane of the hexamer and to the 2-fold axis. Both symmetries can be approximate or exact, in which case they coincide with the
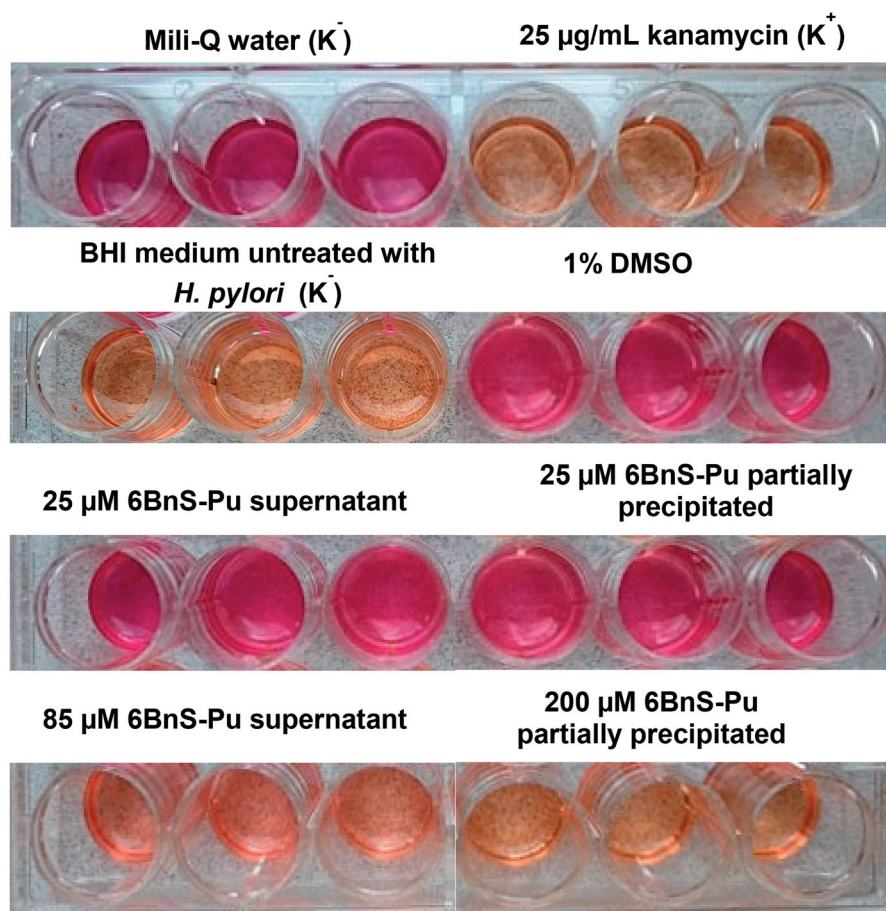
Figure 5. Colour change examples observed in the Christensen's test (see Materials and methods) in wells with *H. pylori* 26695 strain incubated in the presence of various concentrations of **6BnS-Pu**. K⁺ indicates a positive control (25 μg/mL of kanamycin) and K⁻ indicate negative controls as described. The results are presented for three repetitions.

crystallographic symmetry axis. Overall, this means that the enzyme molecules possess an approximate or exact symmetry of the point group 32. Thus, complexes with **6BnS-2Cl-Pu** and **6BnO-2Cl-Pu** crystallise in the cubic space group *P* 2₁ 3 and the asymmetric unit of the crystal is a dimer (Table 1). The whole hexamer is generated by the crystallographic 3-fold axis and possesses an exact 3-fold symmetry (Figure 7(A)).

On the other hand, complexes with compounds **6BnS-Pu** and **2,6-diCl-Pu** crystallise in such a way that the asymmetric unit comprises two hexamers, in the orthorhombic *P* 2₁2₁2₁ and triclinic *P* 1 space group, respectively (Table 1). This propensity of PNPs to crystallise in various space groups with highly different symmetries is known and has been described previously[20,43]. Indeed, the asymmetric unit of the crystal can comprise anything from a single monomer to three hexamers[42].

The monomers themselves are made of a central part with parallel β-sheets surrounded by eight α-helices of varying lengths[21]. Each monomer has one active site located in the cavity close to the terminal α-helix H8 (Figure 7(A)). The active site is completed from one side by the residues His4 and Arg43 from the neighbouring monomer in the dimer. Helix H8 can be in two conformational states: elongated and segmented, which correspond to the *open* and *closed* conformation of the active site. The segmentation of the α-helix H8 occurs around residue Phe219, which undergoes a conformational change, and the last two turns of the helix H8 close the active site pocket[20,21].

The active site in each monomer consists of parts that bind phosphate, pentose, and purine base. The phosphate-binding site is found in the most buried part of the active site, where the phosphate molecule is coordinated by three arginine residues, Arg24, Arg87 from one monomer, and Arg43 from the neighbouring monomer in the dimer. Phosphate molecule is further coordinated with hydrogen bonds to Gly20 and Thr90. Adjacent to the phosphate-binding part is the pentose-binding part surrounded by residues: Arg87, Thr90, Met64, Met180, and Glu181.

Binding of 2,6-substituted purines in the *H. pylori* PNP active site

In all closed active sites, inhibitor, phosphate, and buffer molecules are present (Tris or imidazole in the case of the structure with **2,6-diCl-Pu**). In some of the structures, faint blobs of electron density in the open active sites are also observed, suggesting that in some protein molecules ligands are bound in these sites as well.

Details of ligand binding in the closed active sites of all four structures obtained are shown in Figure 8. The electron density in the closed active site of **6BnS-2Cl-Pu** structure shows the presence of the ligand in the base binding part of the active site, and one molecule of Tris bound in the pentose binding part and a molecule of PO₄. The phenyl arm is positioned towards the exit of the active site and above the plane of the purine base part (Figure 8(A)). **6BnO-2Cl-Pu** shows an analogous way of binding as far as the planar base part is concerned. The difference is in the phenyl arm, which in the case of **6BnO-2Cl-Pu** is positioned below the planar ring of the purine base. The positions of Tris
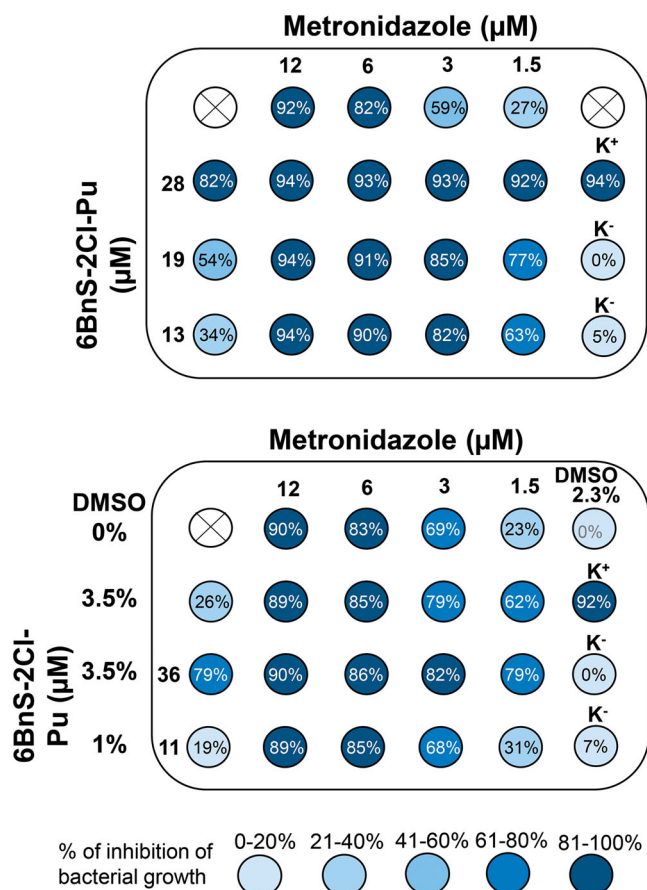
Figure 6. The antibacterial effects of **6BnS-2Cl-Pu**, metronidazole (MTZ), and combination of both against *H. pylori* 26695 strain replication. As solution of **6BnS-2Cl-Pu** contains DMSO (typically roughly 1% per 3 µg/mL of **6BnS-2Cl-Pu**, maximum used was 3.5%), the effect of MTZ solution containing 3.5% DMSO (lower panel, second row), and DMSO alone, 3.5% and 2.3% were also checked. Lower DMSO concentration, 2.3% does not affect *H. pylori* cell culture growth, while 3.5% in this case yields 26% inhibition. The percent inhibition of bacterial growth is described in each well. The white circles with a cross in the middle indicate empty wells, K^+ indicates a positive control (kanamycin 25 µg/mL) and K^- indicate negative controls with water (upper) and BHI medium untreated with *H. pylori* cells (lower). The results are presented as the mean of three repetitions.

and PO_4 molecules are the same as in the previous structure (Figure 8(B)).

Two other purines, **6BnS-Pu** and **2,6-diCl-Pu**, the former lacking chlorine atoms and the latter lacking the benzyl substituent, bind with a purine ring flipped around with respect to the two previous structures (Figure 8). The electron density of the phenyl arm in the structure of **6BnS-Pu** is very poorly visible due to its large conformational mobility. Positions of Tris and PO_4 molecules are the same as in the structures with **6BnS-2Cl-Pu** and **6BnO-2Cl-Pu**. **2,6-diCl-Pu**, which contains two Cl atoms, is very well defined in all twelve open active sites (chain A is shown in Figure 8). In the pentose binding part, one molecule of imidazole is visible and in the place of PO_4, there is one Mg ion coordinated by water molecules and by Arg43. In all active sites, Cys19 is oxidised to cysteic acid (OCS) visible to the far right (Figure 8(D)).

The most important interactions of the protein with ligands, namely, hydrogen bonds, classic and weak, involving carbon, close contacts, and C-H … π interactions are presented in Figure 9 and Table 4. In all four structures, Phe159 is placed on top of the pyrimidine ring and tilted approximately 45 degrees with respect to

the ring plane. The distance from the closest atom to the centre of the C4-C5 bond ranges from 3.2 to 3.7 Å, which is characteristic for C-H···π interaction. Two purine ligands with the best inhibitor properties, namely, **6BnS-2Cl-Pu** and **6BnO-2Cl-Pu** (Table 2), form two strong hydrogen bonds with the protein, N7···$O^{\delta 1}$(Asp204) and N7 … O^{γ}(Ser203). In two other enzyme structures, with weaker inhibitors, **6BnS-Pu** and **2,6-diCl-Pu**, the purine ring is flipped around, so the above contacts are impossible. **6BnS-Pu**, the medium inhibitor (Table 2), forms one strong hydrogen bond N1···$O^{\delta 1}$(Asp204), while in the complex with the weakest inhibitor, **2,6-diCl-Pu**, Asp204 is displaced by the Cl1 atom of the ligand and no strong hydrogen bonds are observed. Hence, the interactions observed in all four structures correlate with the inhibition properties of the ligands.

The upper panel of Figure 10 presents the overlapped positions of all four ligands in the structures of *H. pylori* PNP complexes studied in this report. In the figure legend, the similarities and differences of ligand binding are summarised. The lower panel of this figure compares *H. pylori* PNP complex with **6BnS-2Cl-Pu**, Tris, and PO_4 obtained in this study, to the complex with formycin A and PO_4 (PDB code 6F4X) described previously[20]. Formycin A is the analogue of PNP substrate, adenosine, and exhibits medium competitive *vs.* nucleoside substrate inhibitor properties, as its inhibition constant is $14.0 \pm 1.7\,\mu M$[20]. It can be noted that in both structures, with **6BnS-2Cl-Pu** and with formycin A, the base rings are oriented in the same way, but are slightly tilted, and formycin A is more drawn into the active site because of the covalent bond with the ribose. The molecule of Tris is mimicking the ribose of formycin A with oxygen atoms occupying similar positions. This shows that sufficiently big substituents at positions 2 and 6 of the base secure the proper base orientation in the active site, allowing strong hydrogen bonds with Asp204 and Ser203. However, more space and freedom between the base and the pentose ring, or a base and a molecule mimicking the pentose, are necessary to allow the formation of such bonds and at the same time also strong interaction with the pentose part of the active site. These observations may be used to design nucleoside-like inhibitors, which may also be regarded as bisubstrate inhibitors of the reverse synthetic reaction direction (see reaction scheme in the Introduction). Such compounds may profit from better optimised interactions with the base and pentose binding sites, resulting in most probably stronger binding than observed in the case of formycin and the best inhibitors described in this study.

Conclusion

In this study, we have shown that some purines substituted at positions 2 and/or 6 are effective inhibitors of *H. pylori* PNP, having inhibition constants in the low µM range as well as inhibiting *H. pylori* cell culture growth. Compound with a benzylthio substituent at position 6 of the purine ring exhibits the best inhibition properties. We have determined the X-ray structure of *H. pylori* PNP complexes with each of the purine analogues described above and characterised details of the enzyme-ligand interactions. The strength of binding, characterised by the quality of the electron density maps and the number of contacts with the enzyme are in line with the inhibition properties. These data provide an excellent starting point for designing bisubstrate analogue inhibitors that feature an additional part attached to the 2,6-substituted purine ring, capable of interacting with the pentose-binding site as well. Altogether, we have demonstrated that this class of compounds, based on a novel molecular mechanism and targeting
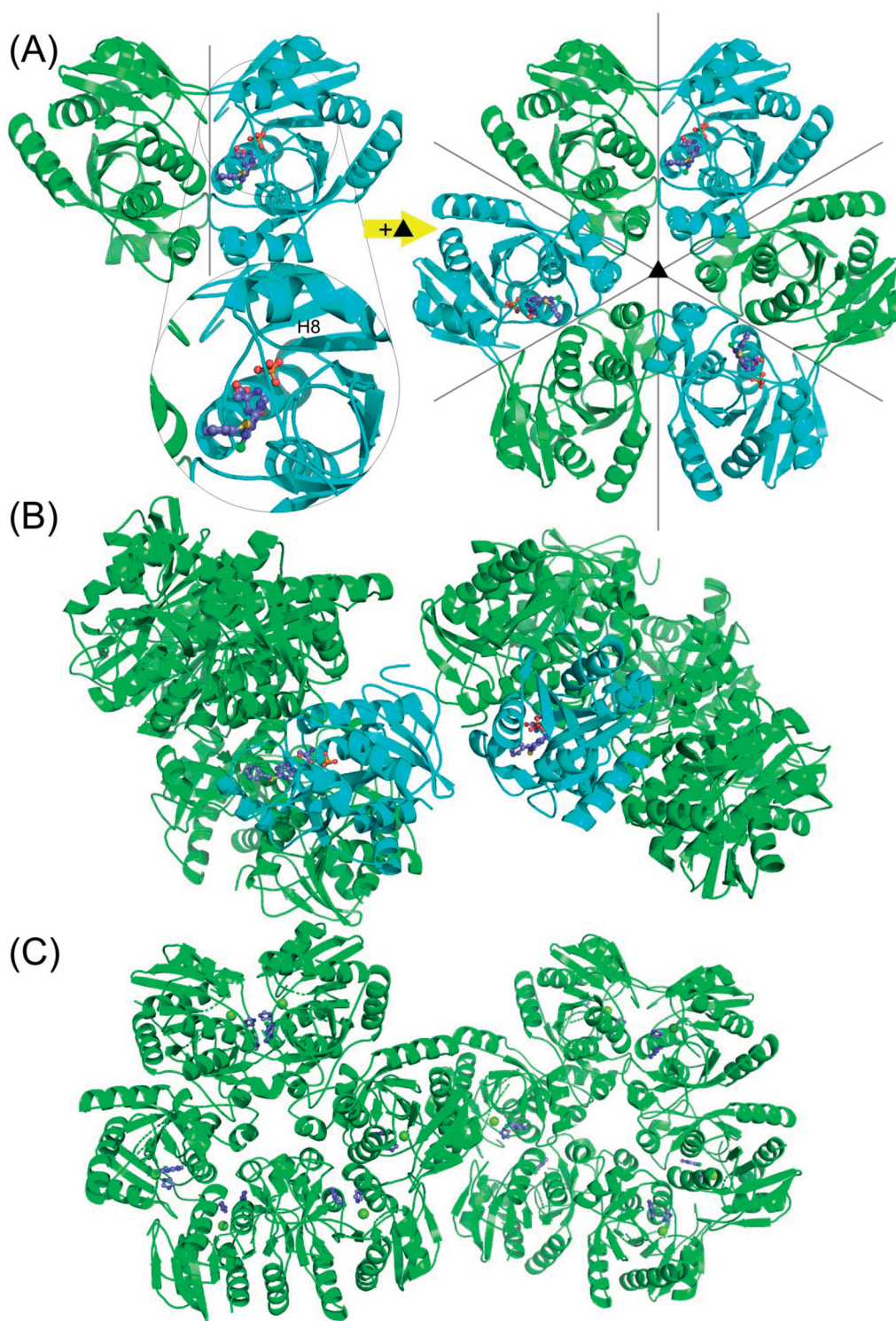
Figure 7. The overall structure of the *H. pylori* PNP complexes with 2,6-substituted purines. (A) Complexes with **6BnS-2Cl-Pu** and **6BnO-2Cl-Pu** crystallise in the cubic space group $P\,2_13$ with two monomers forming a dimer in the asymmetric unit. One of the monomers has the closed (shown in cyan) and one has the open (shown in green) conformation of the active site. The helix which is segmented to close the active site pocket (see text) is designated H8. The complete hexamer is generated by a crystallographic 3-fold axis, and therefore one hexamer has three open and three closed active sites. Ligands are shown in the ball and stick model. (B) In the crystals of PNP with **6BnS-Pu**, two entire hexamers are in the asymmetric unit in the space group $P\,2_12_12_1$, and each hexamer (shown in cyan) has one closed active site. The closed active sites from different hexamers are next to each other in the crystal packing. (C) Complex of PNP with **2,6-diCl-Pu** crystallised also with two hexamers in the asymmetric unit but this time in the $P\,1$ space group. All the monomers are in the open conformation.
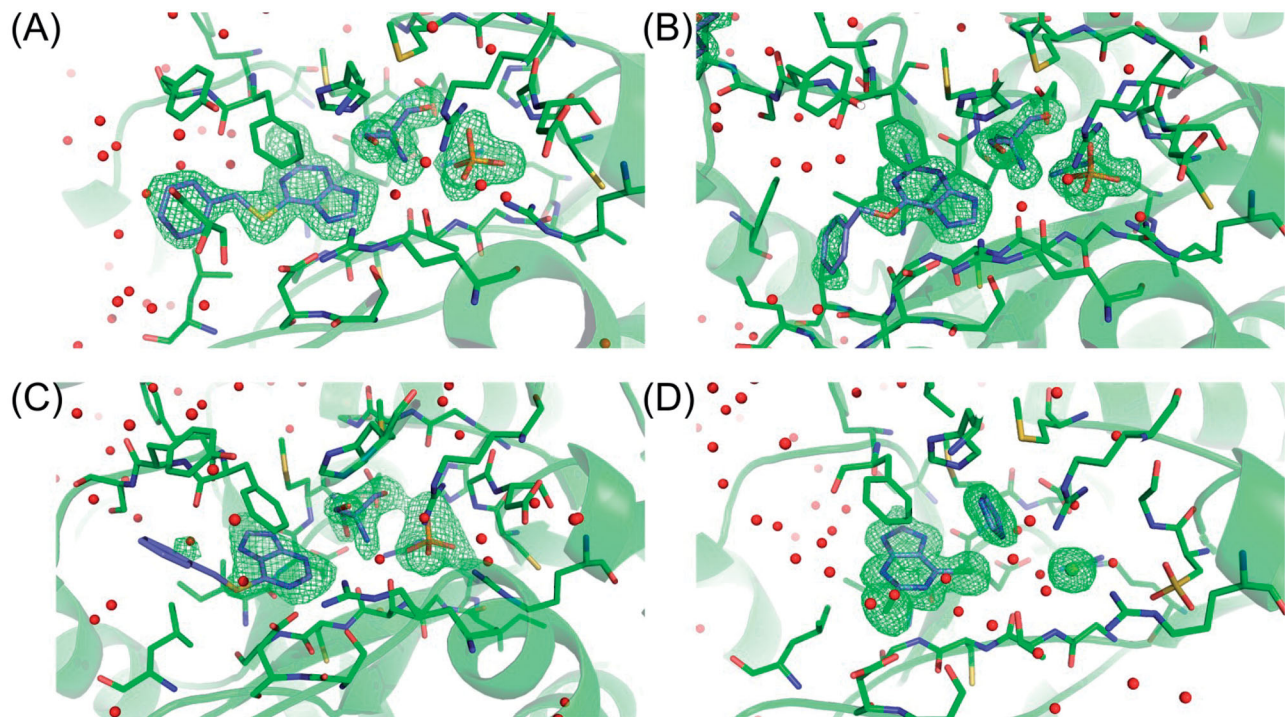
Figure 8. Comparison of closed active sites in all four structures of *H. pylori* PNP with (A) **6BnS-2Cl-Pu**, (B) **6BnO-2Cl-Pu**, (C) **6BnS-Pu**, and (D) **2,6-diCl-Pu**. C atoms of the ligands are shown in violet, protein C atoms in green, and all other atoms in the CPK colours. The figure shows the electron *mFo-DFc* difference map density contoured at 3σ level (shown in green). Electron density only around molecules bound in the active sites is shown. Red spheres represent water molecules, and the green sphere on panel (D) – magnesium atom (from crystallisation mother liquor, see text).
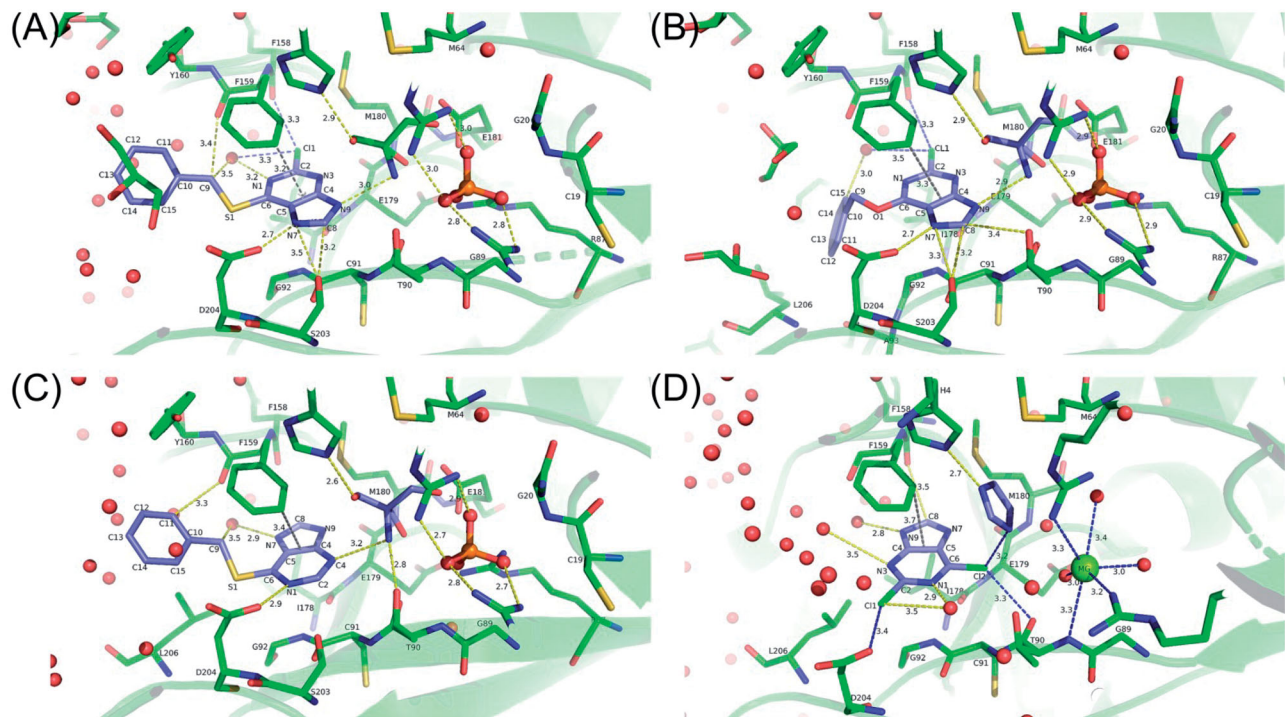

Figure 9. The most important interactions of the protein with ligands in the *H. pylori* PNP complexes with **6BnS-2Cl-Pu** (A), **6BnO-2Cl-Pu** (B), **6BnS-Pu** (C), and **2,6-diCl-Pu** (D). Interactions of ligands under 3.5 Å in length are depicted, hydrogen bonds are shown in yellow, close contacts in blue, and C-H…π interactions are shown in grey. It is visible that in structures with **6BnS-2Cl-Pu** and **6BnO-2Cl-Pu** purine ring is oriented in such a way that the five-membered ring is closer to the viewer, while in the two remaining structures the purine ring is flipped.

Table 4. Hydrogen bonds (marked in bold) and close contacts shorter than 3.5 Å between ligands and active sites residues, observed in structures obtained in this study.

6BnS-2Cl-Pu		6BnO-2Cl-Pu		6BnS-Pu		2,6-diCl-Pu	
N7 … 204(ASP)OD1	2.67	**N7 … 204(ASP)OD1**	2.68	**N1 … 204(ASP)OD1**	2.87	**N9 … 756(HOH)O**	2.78
N9 … 302(TRS)N	3.04	**N9 … 302(TRS)N**	2.94	**N7 … 215(HOH)O**	2.90	**N1 … 663(HOH)O**	2.86
N1 … 192(HOH)O	3.16	C15 … 100(HOH)O	2.99	C11 … 942(HOH)O	3.18	Cl2 … 2(IMD)N1	3.15
C8 … 203(SER)OG	3.23	C8 … 203(SER)OG	3.22	C11 … 159(PHE)O	3.26	Cl2 … 90(THR)O	3.28
CL1 … 158(PHE)O	3.28	CL1 … 158(PHE)O	3.27	**N3 … 301(TRS)N**	3.27	Cl2 … 204(ASP)OD2	3.36
CL1 … 192(HOH)O	3.34	**N7 … 203(SER)OG**	3.31	C9 … 159(PHE)O	3.28	**N3 … 2451(HOH)O**	3.51
C9 … 159(PHE)O	3.38	C8 … 90(THR)OG1	3.38	C9 … 215(HOH)O	3.48	C8 … 158(PHE)O	3.53
C9 … 192(HOH)O	3.44	CL1 … 100(HOH)O	3.49			Cl1 … 663(HOH)O	3.53
N7 … 203(SER)OG	3.47						
C8 … 204(ASP)OD1	3.51						

Atom numbering is given in Scheme S2 in the Supplemental Materials.
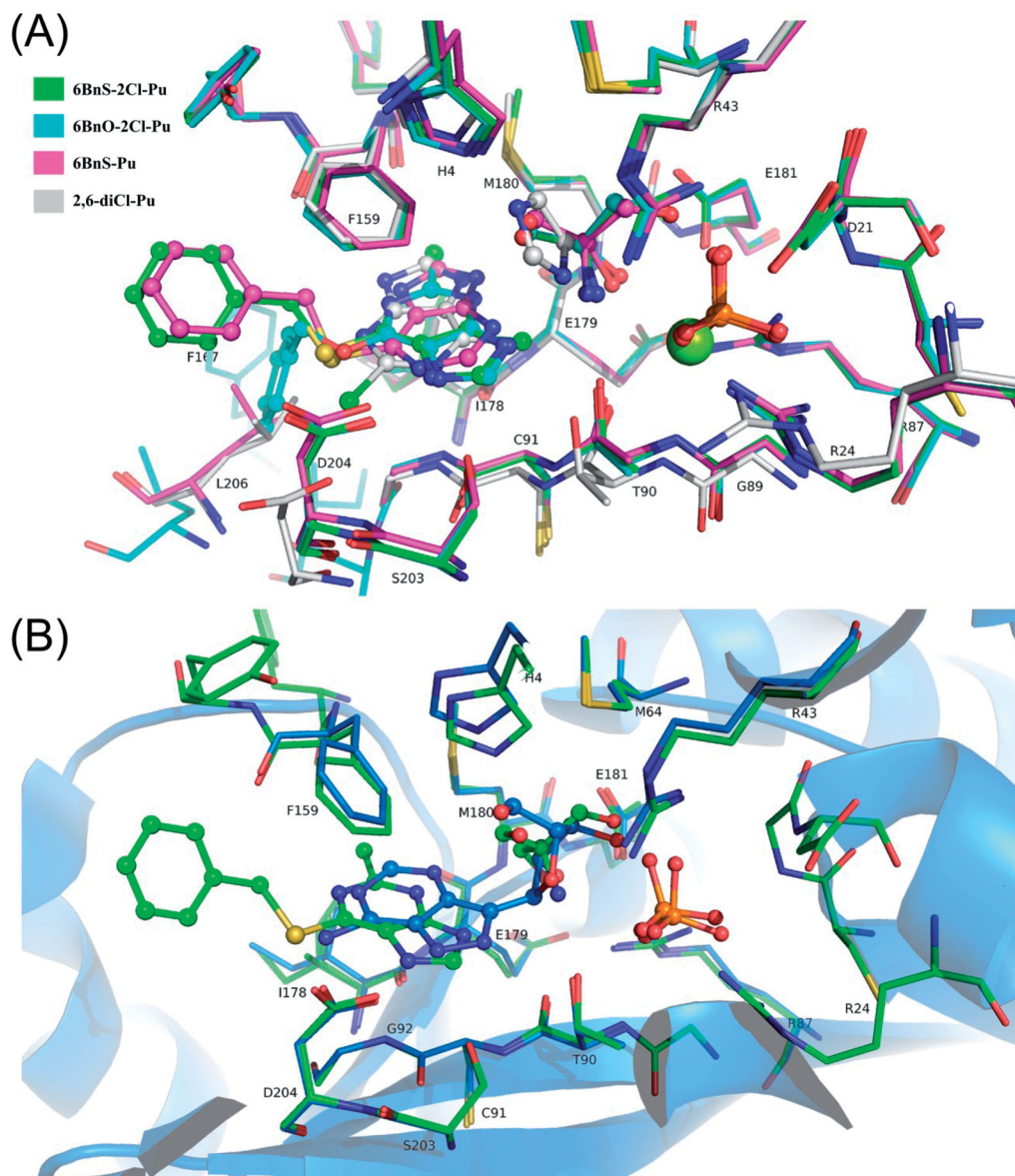
Figure 10. (A) Overlapped positions of ligands in *H. pylori* PNP complexes with **6BnS-2Cl-Pu**, **6BnO-2Cl-Pu**, **6BnS-Pu,** and **2,6-diCl-Pu**. The colour codes of C atoms are shown in the legend, and other atoms have their standard colours. It is visible that the purine ring occupies the base binding pocket. Ligands **6BnS-2Cl-Pu** and **6BnO-2Cl-Pu** have the plane of the ring almost in the identical position, with the chlorine atoms pointing away from the viewer, although their benzyl arms are positioned oppositely. The pentose binding part of the active site is occupied by Tris molecules in all structures except for imidazole in the structure with **2,6-diCl-Pu**. It can be noted that two imidazole nitrogen atoms are positioned close to the positions of one oxygen and one nitrogen atom of Tris molecule to favour hydrogen bond contacts. The phosphate molecules in all structures occupy the same place and are in the same orientation, while in the structure with **2,6-diCl-Pu** a highly coordinated Mg atom is located in this position. It is visible that in the structure with **2,6-diCl-Pu** the second chlorine atom of the ligand displaces the Asp204 side chain. (B) Overlap of the structure with **6BnS-2Cl-Pu** (green) and with formycin A and PO$_4$ (PDB code 6F4X, shown in blue). It can be noted that the base rings are oriented in the same way but are slightly tilted and shifted in relation to each other with formycin A located deeper in the active site because of the covalent bond with the ribose. The molecule of Tris is mimicking the ribose part of formycin A with oxygen atoms occupying similar positions.

the crucial enzyme in the *H. pylori* purine salvage pathway, provides a promising lead structure for designing drugs against this severe pathogen.

Disclosure statement

No potential conflict of interest was reported by the author(s).

ORCID

Marta Narczyk http://orcid.org/0000-0002-7844-7262
Marta Ilona Wojtyś http://orcid.org/0000-0003-3850-7598
Ivana Leščić Ašler http://orcid.org/0000-0002-0826-7493
Biserka Žinić http://orcid.org/0000-0002-1536-7142
Elżbieta Katarzyna Jagusztyn-Krynicka http://orcid.org/0000-0003-0484-9290
Zoran Štefanić http://orcid.org/0000-0002-3486-4291
Agnieszka Bzowska http://orcid.org/0000-0002-3976-429X

References

1. Marshall BJ, Warren JR. Unidentified curved bacilli in the stomach of patients with gastritis and peptic ulceration. Lancet 1984;1:1311–5.
2. Makola D, Peura DA, Crowe SE. *Helicobacter pylori* infection and related gastrointestinal diseases. J Clin Gastroenterol 2007;41:548–58.
3. Robinson K, Atherton JC. The spectrum of *Helicobacter*-mediated diseases. Annu Rev Pathol Mech Dis 2021;16:123–44.
4. Falco MDE, Lucariello A, Iaquinto S, et al. Molecular mechanisms of *Helicobacter pylori* pathogenesis. J Cell Physiol 2015;230:1702–7.
5. Cover TL. *Helicobacter pylori* diversity and gastric cancer risk. mBio 2016;7:1–9.
6. Schistosomes, liver flukes and Helicobacter pylori. IARC Working Group on the Evaluation of Carcinogenic Risks to Humans. Lyon, 7–14 June 1994. IARC Monogr Eval Carcinog Risks Hum 1994;61:1–241.
7. Georgopoulos S, Papastergiou V. An update on current and advancing pharmacotherapy options for the treatment of *H. pylori* infection. Expert Opin Pharmacother 2021;22:729–41.
8. De Freitas LC. WHO (2017) Global priority list of antibiotic-resistant bacteria to guide research, discovery, and development of new antibiotics. Cad Pesqui 2013;43:348–65.
9. Roszczenko-Jasińska P, Wojtyś MI, Jagusztyn-Krynicka EK. *Helicobacter pylori* treatment in the post-antibiotics era-searching for new drug targets. Appl Microbiol Biotechnol 2020;104:9891–905.
10. Campestre C, De Luca V, Carradori S, et al. Carbonic anhydrases: new perspectives on protein functional role and inhibition in *Helicobacter pylori*. Front Microbiol 2021;12:1–12.
11. Ullman B, Carter D. Hypoxanthine-guanine phosphoribosyltransferase as a therapeutic target in protozoal infections. Infect Agents Dis 1995;4:29–40.
12. El Kouni MH. Potential chemotherapeutic targets in the purine metabolism of parasites. Pharmacol Ther 2003;99:283–309.
13. de Koning HP, Bridges DJ, Burchmore RJS. Purine and pyrimidine transport in pathogenic protozoa: from biology to therapy. FEMS Microbiol Rev 2005;29:987–1020.
14. Hyde JE. Fine targeting of purine salvage in cryptosporidium parasites. Trends Parasitol 2008;24:336–9.
15. Berg M, Van der Veken P, Goeminne A, et al. Inhibitors of the purine salvage pathway: a valuable approach for antiprotozoal chemotherapy? Curr Med Chem 2010;17:2456–81.
16. Evans GB, Tyler PC, Schramm VL. Immucillins in infectious diseases. ACS Infect Dis 2018;4:107–17.
17. Liechti G, Goldberg JB. *Helicobacter pylori* relies primarily on the purine salvage pathway for purine nucleotide biosynthesis. J Bacteriol 2012;194:839–54.
18. Il'icheva IA, Polyakov KM, Mikhailov SN. Strained conformations of nucleosides in active sites of nucleoside phosphorylases. Biomolecules 2020;10:552.
19. Koellner G, Luić M, Shugar D, et al. Crystal structure of the ternary complex of *E. coli* purine nucleoside phosphorylase with formycin B, a structural analogue of the substrate inosine, and phosphate (sulphate) at 2.1 A resolution. J Mol Biol 1998;280:153–66.
20. Narczyk M, Bertoša B, Papa L, et al. *Helicobacter pylori* purine nucleoside phosphorylase shows new distribution patterns of open and closed active site conformations and unusual biochemical features. FEBS J 2018;285:1305–25.
21. Štefanić Z, Mikleušević G, Luić M, et al. Structural characterization of purine nucleoside phosphorylase from human pathogen *Helicobacter pylori*. Int J Biol Macromol 2017;101:518–26.
22. Bzowska A, Magnowska L, Kazimierczuk Z. Synthesis of 6-aryloxy- and 6-arylalkoxy-2-chloropurines and their interactions with purine nucleoside phosphorylase from *Escherichia coli*. Z Naturforsch C 1999;54:1055–67.

23. Jones JW, Robins RK. Purine nucleosides. III. Methylation studies of certain naturally occurring purine nucleosides. J Am Chem Soc 1963;85:193–201.

24. Schrader WP, Stacy AR, Pollara B. Purification of human erythrocyte adenosine deaminase by affinity column chromatography. J Biol Chem 1976;251:4026–32.

25. Bzowska A, Kazimierczuk Z, Seela F. 7-deazapurine 2′-deoxy-ribofuranosides are noncleavable competitive inhibitors of Escherichia coli purine nucleoside phosphorylase (PNP). Acta Biochim Pol 1998;45:755–68.

26. Bzowska A, Kazimierczuk Z. 2-Chloro-2′-deoxyadenosine (cladribine) and its analogues are good substrates and potent selective inhibitors of Escherichia coli purine-nucleoside phosphorylase. Eur J Biochem 1995;233:886–90.

27. Kalckar HM, Shafran W. Differential spectrophotometry of purine compounds by means of specific enzymes; Determination of hydroxypurine compounds. J Biol Chem 1947;167:429–43.

28. Kulikowska E, Bzowska A, Wierzchowski J, Shugar D. Properties of two unusual, and fluorescent, substrates of purine-nucleoside phosphorylase: 7-methylguanosine and 7-methylinosine. Biochim Biophys Acta (BBA)/Protein Struct Mol 1986;874:355–63.

29. Bzowska A, Kulikowska E, Shugar D. Properties of purine nucleoside phosphorylase (PNP) of mammalian and bacterial origin. Z Naturforsch C J Biosci 1990;45:59–70.

30. Segel IH, Enzyme kinetics: behavior and analysis of rapid equilibrium and steady-state enzyme systems. Vol. 2. New York, NY: John Wiley Sons; 1993.

31. Copeland RA, Enzymes. New York, NY: John Wiley & Sons, Inc.; 2000.

32. Irie Y, Tateda K, Matsumoto T, et al. Antibiotic MICs and short time-killing against Helicobacter pylori: therapeutic potential of kanamycin. J Antimicrob Chemother 1997;40:235–40.

33. Chowers MY, Keller N, Tal R, et al. Human gastrin: a Helicobacter pylori-specific growth factor. Gastroenterology 1999;117:1113–8.

34. Knezevic P, Aleksic Sabo V, Simin N, et al. A colorimetric broth microdilution method for assessment of Helicobacter pylori sensitivity to antimicrobial agents. J Pharm Biomed Anal 2018;152:271–8.

35. Krzyżek P, Franiczek R, Krzyżanowska B, et al. In vitro activity of 3-bromopyruvate, an anticancer compound, against antibiotic-susceptible and antibiotic-resistant Helicobacter pylori strains. Cancers (Basel) 2019;11:229.

36. EUCAST. Breakpoint tables for interpretation of MICs and zone diameters. Version 11.0, 2021. Available from: http://www.eucast.org.

37. Pillai SK, Eliopoulos GM, Moellering RC. Antimicrobial combinations. Antibiotics in laboratory medicine. Philadelphia, PA: Wolters Kluwer Health; 2005:365–409.

38. Kabsch W. Xds. Acta Crystallogr D Biol Crystallogr 2010;66:125–32.

39. Vagin A, Teplyakov A. MOLREP: an automated program for molecular replacement. J Appl Crystallogr 1997;30:1022–5.

40. Liebschner D, Afonine PV, Baker ML, Bunkóczi G, et al. Macromolecular structure determination using X-rays, neutrons and electrons: recent developments in phenix. Acta Crystallogr D Struct Biol 2019;75:861–77.

41. Schrödinger LLC. The {PyMOL} molecular graphics system, Version~1.8. 2015.

42. Mikleušević G, Štefanić Z, Narczyk M, et al. Validation of the catalytic mechanism of Escherichia coli purine nucleoside phosphorylase by structural and kinetic studies. Biochimie 2011;93:1610–22.

43. Luić M, Štefanić Z. Can crystal symmetry and packing influence the active site conformation of homohexameric purine nucleoside phosphorylases? Croat Chem Acta 2016;89:197–202.